

# Neural network-motivated regularity analysis of inverse problems and application to inverse scattering

Mahadevan Ganesh <sup>\*</sup>, Stuart C. Hawkins <sup>†</sup>, Darko Volkov <sup>‡</sup>

February 12, 2025

## Abstract

We derive Lipschitz regularity estimates for an approximate inverse of a general compact operator that depends non-linearly on a vector parameter. The regularity estimates are motivated by the desire to develop neural networks (NN) that compute that approximate inverse and the convergence of the NNs follows from the Lipschitz regularity estimates. Such compact operators arise in inverse wave scattering applications with unbounded domains, and we illustrate our theory by showing that the particular assumptions of our regularity analysis hold for the problem of identifying cracks from far-field data. Numerical results using a NN for parameter recovery demonstrate the accuracy, efficiency and robustness of our approach.

**MSC 2020 Mathematics Subject Classification:** 35R30, 35J67, 45Q05, 47N40, 68T07.

**Keywords:** Nonlinear inverse problems, Regularity estimates, Inverse scattering, Neural networks

## Acknowledgement

SCH and MG gratefully acknowledge the support of the Australian Research Council (ARC) Discovery Project Grant (DP220102243). MG is supported by the Simons Foundation through Grant No. 5188. DV is supported by the Simons Foundation through Grant MPS-TSM-00007534.

## 1 Introduction

This article focuses on proving regularity estimates for the inverse of a general compact operator depending non-linearly on a vector parameter. These regularity estimates hold on

---

<sup>\*</sup>Department of Applied Mathematics and Statistics, Colorado School of Mines, Golden, CO, USA

<sup>†</sup>Department of Mathematical and Physical Sciences, Macquarie University, Sydney, NSW 2109, Australia

<sup>‡</sup>Department of Mathematical Sciences, Worcester Polytechnic Institute, Worcester, MA 01609. Corresponding author email: darko@wpi.edu.

subspaces in the span of a finite number of singular vectors if two conditions  $(U1)$ - $(U2)$ , stated in section 2, are verified. We give generic examples to illustrate the two conditions  $(U1)$ - $(U2)$  in section 2.2. Condition  $(U1)$  is just an injectivity condition while, as discussed in section 2.3, condition  $(U2)$  relates to the inverse function theorem. After that, we provide a formal proof of the regularity results. The proof relies on functional analysis techniques such as compactness, weak and strong convergence, and local continuity of parameter dependent spectral projectors for compact symmetric operators. These spectral projectors are known to be not necessarily globally continuous with regard to that parameter [12]: this is arguably the main challenge in our proof. Our main regularity result is stated in Theorem 3.1. Although we proved a result similar to Theorem 3.1 in an earlier study [21], there are substantial differences between these two results. The study [21] pertained specifically to integral operators. The results covered here are more general. Moreover, the lower bound provided here in Theorem 3.1 is sharper, depending both on the nonlinear parameter and on linear terms. Finally, the proof technique adopted here is quite different. A first result is shown in the finite dimensional case in section 3.1. It is then involved in tackling the infinite dimensional case by use of maps between singular spaces and a fixed finite dimensional space. These maps are proved to be locally  $C^1$  in the nonlinear parameter thanks to conditions  $(U1)$ - $(U2)$ .

In section 4, we apply our theory to an example in inverse scattering. In this example, the forward model is governed by the Helmholtz equation in an unbounded region. The inverse scattering problem consists of identifying a crack in the propagation medium, which is done by first training a neural network. This example is very specific, however, we strongly believe that the method introduced here could work just as well in other propagating wave cases as long as some integral formulation is possible such as in [3, 7, 8, 14, 17].

Section 5 of this paper covers computational aspects involved in the specific application to inverse scattering that we consider. These computations rely on a solid mathematical background. Indeed, first, the general requirements from section 3 guaranteeing regularity are proved to hold for the inverse problem at hand in section 4. Second, the gap between regularity for this continuously defined inverse problem and regularity for its discrete analog was bridged in [21, Theorem 4.2]. And third, precise convergence results were proved for approximations of regular functions by neural networks [15, 25, 5]. In particular, [5, Corollary 5.4] gives an explicit bound on the number of nodes of a deep neural network with  $n$  nodes approximating a Lipschitz continuous function on  $[0, 1]^d$ . The number of nodes does not grow faster than  $O(n^d)$  for an approximation in  $L^\infty$  norm bounded above by  $O(n^{-1})$ .

The simulations presented in section 5 comprise three stages. First, data for training the NN is built up and stored. Second, the NN is trained on that data. Third, the accuracy and the computational speed of the NN is tested on entirely new data. This new data is randomly selected from four kinds:

1. **Plane wave excitation with unknown incident direction:** The crack is excited by an incoming plane wave.
2. **Internal source excitation with unknown source location:** The crack is excited by a point-source located between the crack and the scattered wave measurement points.

3. **External source excitation with unknown incident direction:** The crack is excited by a point-source located outside a circle containing the scattered wave measurement points.
4. **Arbitrarily constructed forcing term:** The forcing term is an artificial function defined on the crack.

The fourth case is particularly relevant for modeling the destabilization of cracks in materials under mechanical strain. Our results demonstrate that the NN can accurately compute the nonlinear parameter describing the geometry of the crack *regardless of the forcing term or specific excitation method (plane wave, internal/external source, or artificial forcing function)*, as predicted by the theory. Additionally, the NN achieves remarkable computational efficiency, being orders of magnitude faster than traditional minimization methods for solving nonlinear inverse problems. It also exhibits robustness to noise perturbations, ensuring stability under realistic conditions. Since the focus of this work is the regularity analysis of a large class of inverse problems, the numerical example presented here features a small number of parameters. In a future study, we shall consider more complex geometries and accordingly, larger numbers of parameters.

## 2 Preliminaries

Our theoretical framework in Section 3.1 to establish Lipschitz regularity under a general theoretical framework is based on the following nomenclature.

### 2.1 Abstract framework and assumptions

Let

- $K$  denote the field  $\mathbb{R}$  or  $\mathbb{C}$ ;
- $E$  and  $F$  be two Hilbert spaces over  $K$ ;
- $A_m$  be a compact linear operator from  $E$  to  $F$  depending on a vector parameter  $m$ ;
- the vector parameter  $m$  be in a compact set  $\mathcal{B}$  of  $\mathbb{R}^p$ ; and
- the function  $m \mapsto A_m$  be of class  $C^1$  in  $\mathcal{B}'$ , an open neighborhood of  $\mathcal{B}$ .

For establishing the Lipschitz regularity of the inverse map  $A_m u \mapsto (m, u)$ , for all  $m \in \mathcal{B}$  and  $u \in E$ , we need the following two injectivity assumptions:

- (U1) For any  $m, m'$  in  $\mathcal{B}$ , for any  $u, v$  in  $E$ , if  $u \neq 0$  and  $A_m u = A_{m'} v$  then  $m = m'$  and  $u = v$ .
- (U2) For  $q$  in  $\mathbb{R}^p$  with  $|q| = 1$ , denote  $\partial_q A_m$  the derivative of  $A_m$  in  $m$  in the direction of  $q$ . The linear operator  $T : E \times E \rightarrow F$ ,  $T(u, v) = \partial_q A_m u + A_m v$  is injective.

Clearly, (U1) is a necessary and sufficient condition for the inverse map  $A_m u \mapsto (m, u)$  to be defined on the set  $\{A_m u : m \in \mathcal{B}, u \neq 0 \in E\}$ . We will explain further how condition (U2) relates to the inverse function theorem. If  $E$  is infinite-dimensional, then the inverse map  $A_m u \mapsto (m, u)$  is unbounded. Accordingly, we will only consider in that case the map  $A_m u \mapsto (m, u)$  on subsets of  $\{A_m u : m \in \mathcal{B}, u \neq 0 \in E\}$ . These subsets will be defined using  $m$  dependent singular subspaces of  $A_m$ . These spaces can be computed in practical applications, as demonstrated further.

## 2.2 Generic examples

Before proceeding with statements of regularity results and their proof, we provide generic examples illustrating how assumptions (U1)-(U2) can hold in practice. Later, in section 4.2, we will verify assumptions (U1)-(U2) for a class of wave propagation models.

### Generic Example-1 (Finite Dimensional spaces $E$ and $F$ ):

Choose  $\mathcal{B} = [1, 2]^2$ ,  $E = \mathbb{R}^n$  with its natural basis  $e_1, \dots, e_n$ ,  $F = \mathbb{R}^{3n}$  with its natural basis  $f_1, \dots, f_{3n}$ . For  $m = (m_1, m_2)$  in  $\mathcal{B}$  for our first generic example, define  $A_m$  by setting for  $j = 1, \dots, n$ ,

$$A_m e_j = m_1 f_j + m_2 f_{j+n} + m_2^2 f_{j+2n}.$$

To verify (U1) for this example, let  $u, v \in E$  with  $u = \sum_{j=1}^n u_j e_j$ ,  $v = \sum_{j=1}^n v_j e_j$  such that  $u \neq 0$ . Let  $m, m' \in \mathcal{B}$ . Assume that  $A_m u = A_{m'} v$ . Then for some  $k$  in  $\{1, \dots, n\}$ ,  $u_k \neq 0$  and  $m_1 u_k = m'_1 v_k$ ,  $m_2 u_k = m'_2 v_k$ , and  $m_2^2 u_k = m_2'^2 v_k$ . This implies that  $m_2 = m_2'$ , so  $u_k = v_k$  and  $m_1 = m_1'$ .  $u = v$  easily follows from there.

Next to verify the assumption (U2), we let  $q = (\cos \alpha, \sin \alpha)$  and assume that for  $u = \sum_{j=1}^n u_j e_j$ ,  $v = \sum_{j=1}^n v_j e_j$  in  $E$  and some  $m$  in  $\mathcal{B}$ ,  $\partial_q A_m u + A_m v = 0$ . Then for  $j = 1, \dots, n$ ,

$$\begin{aligned} (\cos \alpha) u_j + m_1 v_j &= 0, \\ (\sin \alpha) u_j + m_2 v_j &= 0, \\ 2m_2 (\sin \alpha) u_j + m_2^2 v_j &= 0. \end{aligned}$$

If  $\sin \alpha = 0$ , then the first two equations imply  $u_j = v_j = 0$ . If  $\sin \alpha \neq 0$ , then the last two equations imply  $u_j = v_j = 0$ . In all cases, we found that  $\partial_q A_m + A_m$  is injective on  $E \times E$ .

### Generic Example-2 (Infinite Dimensional spaces $E$ and $F$ ):

For this example, again we choose the parameter set to  $\mathcal{B} = [1, 2]^2$ . Let  $E$  an infinite dimensional Hilbert space and  $\{e_n : n \geq 1\}$  a Hilbert basis of  $E$ . Let  $F$  be another infinite dimensional Hilbert space and  $\{f_n : n \geq 1\}$  a Hilbert basis of  $F$ . For  $m = (m_1, m_2)$  in  $\mathcal{B}$  we define  $A_m$  by setting for  $n \geq 1$

$$A_m e_n = \frac{m_1}{n} f_{3n} + \frac{m_2}{n} f_{3n+1} + \frac{m_2^2}{n} f_{3n+2}.$$

Note that this definition ensures that  $A_m$  is compact. Similar to calculations in the previous Example-1, it can be shown that the assumptions (U1)-(U2) also hold for this example.

## 2.3 Comments on the conditions (U1)–(U2)

Note that (U1) implies in particular that  $A_m$  is injective for all  $m$  in  $\mathcal{B}$ , while (U2) implies in particular that  $\partial_q A_m$  is injective for all  $q$  in  $\mathbb{R}^p$ ,  $q = 1$ , and  $m$  in  $\mathcal{B}$ .

Condition (U2) can be related to the inverse function theorem. Indeed, consider the function

$$\mathcal{A} : \mathcal{B}' \times E \rightarrow F \quad (1)$$

$$(m, u) \mapsto A_m u. \quad (2)$$

It is of class  $C^1$  according to the assumptions in Proposition 3.1. If  $(m_0, u_0)$  is an interior point of  $\mathcal{B} \times E$ , if the Jacobian  $J$  of  $\mathcal{A}$  at  $(m_0, u_0)$  is injective on  $\mathbb{R}^p \times E$  then  $\mathcal{A}$  has a  $C^1$  inverse in a neighborhood of  $(m_0, u_0)$ .

For simplicity, let us assume in this paragraph that  $K = \mathbb{R}$ . Let  $e_1, \dots, e_p$  be the natural basis of  $\mathbb{R}^p$  and  $f_1, \dots, f_s$  be a basis of  $E$ .  $J$  is injective if and only if for all non-zero vectors  $(a_1, \dots, a_p, b_1, \dots, b_s)$  in  $\mathbb{R}^{p+s}$ ,

$$(a_1 \partial_{e_1} A_{m_0} + \dots + a_p \partial_{e_p} A_{m_0}) u_0 + A_{m_0} (b_1 f_1 + \dots + b_s f_s) \neq 0. \quad (3)$$

If (U2) holds and  $u_0 \neq 0$ , it is clear that (3) holds. Now assume (U2) does not hold. Then there is  $q$  in  $\mathbb{R}^p$  with  $|q| = 1$ ,  $q = (q_1, \dots, q_p)$ ,  $m_0$  in  $\mathcal{B}$  and  $(u_0, v_0) \neq (0, 0)$  in  $E \times E$  such that  $\partial_q A_m u + A_m v = 0$ . Accordingly

$$(q_1 \partial_{e_1} A_{m_0} + \dots + q_p \partial_{e_p} A_{m_0}) u_0 + A_{m_0} v_0 = 0. \quad (4)$$

If  $u_0 = 0$ , then  $v_0 \neq 0$ : this shows that condition (U1) does not hold. If  $u_0 \neq 0$ , this shows that (3) does not hold.

## 3 Lipschitz regularity results for the inverse of $A_m$

We first prove the regularity result with finite-dimensional space setting, and subsequently prove the regularity of the inverse of  $A_m$  defined on an infinite dimensional Hilbert space  $E$ .

### 3.1 regularity proof for the finite-dimensional case

**Proposition 3.1.** *Consider the framework and assumptions in section 2.1. In addition assume  $E$  is finite-dimensional. Then there is a positive constant  $C$  such that for all  $m, m'$  in  $\mathcal{B}$  and  $u, v$  in  $E$ ,*

$$\|A_m u - A_{m'} v\| \geq C(|m - m'| \|v\| + \|u - v\|). \quad (5)$$

**Proof:** We note that since  $E$  is finite-dimensional,  $\mathcal{B}$  is compact and  $A_m$  and  $\partial_q A_m$  are continuous in  $m$ , according to (U2), there is a constant  $\alpha > 0$  such that

$$\|\partial_q A_m u + A_m v\| \geq \alpha(\|u\| + \|v\|), \quad (6)$$

for all  $m$  in  $B$ , all  $q$  in  $\mathbb{R}^p$  with  $|q| = 1$ , and all  $u, v$  in  $E$ .

Arguing by contradiction assume that there are two sequences  $m_n, m'_n$  in  $\mathcal{B}$  and two sequences  $u_n, v_n$  in  $E$  such that

$$\|A_{m_n}u_n - A_{m'_n}v_n\| \leq \frac{1}{n}(|m_n - m'_n|\|v_n\| + \|u_n - v_n\|), \quad (7)$$

while  $|m_n - m'_n|\|v_n\| + \|u_n - v_n\| \neq 0$ . By compactness we can assume that  $m_n$  converges to some  $m$  in  $\mathcal{B}$  and  $m'_n$  converges to some  $m'$  in  $\mathcal{B}$ .

If we assume that  $\|v_n\| = 0$ , we contradict (6).

If we assume that  $\|u_n - v_n\| = 0$ , then

$$\|(A_{m_n} - A_{m'_n})u_n\| \leq \frac{1}{n}|m_n - m'_n|\|u_n\|.$$

After extracting a subsequence we may assume that  $\frac{u_n}{\|u_n\|}$  converges to  $\phi \neq 0$  in  $E$ . If  $m \neq m'$ , we obtain at the limit  $(A_m - A_{m'})\phi = 0$ , contradicting (U1). If  $m = m'$ , then after extracting a subsequence we may assume that  $\frac{m_n - m'_n}{|m_n - m'_n|}$  converges to some  $q$  in  $\mathbb{R}^p$ . At the limit we obtain  $\partial_q A_m \phi = 0$  contradicting (6).

If we assume that  $|m_n - m'_n| = 0$  then  $\|A_{m_n}(u_n - v_n)\| \leq \frac{1}{n}\|u_n - v_n\|$  again contradicting (6).

Altogether, after possibly extracting a subsequence we can assume that  $\|v_n\| \neq 0$ ,  $\|u_n - v_n\| \neq 0$ , and  $|m_n - m'_n| \neq 0$ . We set

$$\omega_n = \frac{|m_n - m'_n|\|v_n\|}{|m_n - m'_n|\|v_n\| + \|u_n - v_n\|},$$

and by (7) we find as  $n \rightarrow \infty$  that

$$\omega_n \frac{A_{m_n} - A_{m'_n}}{|m_n - m'_n|} \frac{v_n}{\|v_n\|} + (1 - \omega_n) A_{m_n} \frac{u_n - v_n}{\|u_n - v_n\|} \rightarrow 0. \quad (8)$$

After extracting subsequences, we may assume that  $\omega_n$  converges to some  $\omega$  in  $[0, 1]$  and  $\frac{v_n}{\|v_n\|}$  converges to some  $\phi$  in  $E$  and  $\frac{u_n - v_n}{\|u_n - v_n\|}$  converges to some  $\psi$  in  $E$  with  $\|\phi\| = \|\psi\| = 1$ . Two cases arise. In the first case  $m \neq m'$ . In that case we find at the limit

$$\omega \frac{A_m - A_{m'}}{|m - m'|} \phi + (1 - \omega) A_m \psi = 0. \quad (9)$$

This contradicts (U1) since  $m \neq m'$  and  $\|\phi\| = \|\psi\| = 1$ . In the second case  $m = m'$ . After extracting a subsequence we may assume that  $\frac{m_n - m'_n}{|m_n - m'_n|}$  converges to some  $q$  in  $\mathbb{R}^p$  and we write

$$\frac{A_{m_n} - A_{m'_n}}{|m_n - m'_n|} = \int_0^1 \nabla_m A_{m'_n + t(m_n - m'_n)} \frac{m_n - m'_n}{|m_n - m'_n|} dt.$$

Since  $A_m$  is  $C^1$  in  $m$ , as  $n \rightarrow \infty$  we find from (8)

$$\omega \partial_q A_m \phi + (1 - \omega) A_m \psi = 0.$$

As  $\|\phi\| = \|\psi\| = 1$ , this contradicts (U2).  $\square$

**Remark 3.1.** Since  $m$  and  $m'$  as well as  $u$  and  $v$  can be switched in regularity estimate (5), we can equivalently write that for some constant  $C$ ,

$$\|A_m u - A_{m'} v\| \geq C(|m - m'|(\|u\| + \|v\|) + \|u - v\|),$$

for all  $m, m'$  in  $B$  and  $u, v$  in  $E$ .

**Remark 3.2.** We show that conditions (U1), (U2) are necessary for Lipschitz regularity of the inverse operator estimate (5) to hold. Condition (U1) clearly follows from (5). To show (U2) from (5), fix  $m$  and  $u$  set  $m' = m - \frac{q}{n}$  and  $u - v = \frac{w}{n}$ . Let  $n \rightarrow \infty$  to obtain

$$\|\partial_q A_m u + A_m w\| \geq C(\|u\| + \|w\|),$$

showing (U2).  $\square$ .

### 3.2 The infinite-dimensional case: Projections on finite-dimensional singular spaces

We again consider the abstract framework and assumptions in section 2.1, with  $E$  may be infinite-dimensional. We introduce parameter dependent orthogonal projections and first prove the regularity estimates on the range of the projections.

For  $m$  in  $\mathcal{B}$  let

$$\lambda_1^2(m) > \dots > \lambda_N^2(m) > \dots$$

be the distinct ordered eigenvalues of  $A_m^* A_m$ . Fix  $m_1$  in  $\mathcal{B}$  and let  $P_{m_1}$  be the orthogonal projection on the sum of the eigenspaces of  $A_{m_1}^* A_{m_1}$  corresponding to the eigenvalues  $\lambda_1^2(m_1), \dots, \lambda_N^2(m_1)$ . Let  $\mathcal{C}_1$  be the circle in the complex plane centered at the origin with radius  $\max_{m \in \mathcal{B}} \|A_m^* A_m\| + 1$ , and  $\mathcal{C}_2$  be the circle centered at the origin with radius  $\frac{\lambda_N^2(m_1) + \lambda_{N+1}^2(m_1)}{2}$ .

For  $m$  near  $m_1$  define [12],

$$P_{m,1} = \frac{1}{2i\pi} \int_{\mathcal{C}_1} (zI - A_m^* A_m)^{-1} dz - \frac{1}{2i\pi} \int_{\mathcal{C}_2} (zI - A_m^* A_m)^{-1} dz. \quad (10)$$

Note that for  $m$  near  $m_1$ ,  $P_{m,1}$  is also an orthogonal projection on the sum of the eigenspaces of  $A_m^* A_m$  corresponding to the eigenvalues greater than  $\frac{\lambda_N^2(m_1) + \lambda_{N+1}^2(m_1)}{2}$ . Formula (10) can be used to prove that  $m \mapsto P_{m,1}$  is a  $C^1$  function in a connected neighborhood  $V_{m_1}$  of  $m_1$ . Necessarily,  $s_1 = \dim R(P_{m,1})$  is constant in  $V_{m_1}$  by continuity of the trace.

Next we show that after possibly shrinking  $V_{m_1}$  there is a linear bijection  $\varphi_{m,1} : K^{s_1} \rightarrow R(P_{m,1})$  such that  $m \mapsto \varphi_{m,1}$  is a  $C^1$  function in  $V_{m_1}$ . Indeed, let  $v_{1,1}, \dots, v_{1,s_1}$  be an orthonormal basis of  $R(P_{m_1})$ . The matrix  $\langle P_{m_1,1} v_{1,i}, P_{m_1,1} v_{1,j} \rangle_{1 \leq i, j \leq s_1}$  is the identity matrix since  $P_{m_1,1} v_{1,i} = v_{1,i}$ . By continuity,  $\langle P_{m,1} v_{1,i}, P_{m,1} v_{1,j} \rangle_{1 \leq i, j \leq s_1}$  is invertible for  $m$  near  $m_1$ , proving that  $P_{m,1} v_{1,1}, \dots, P_{m,1} v_{1,s_1}$  is a basis of  $R(P_{m,1})$  since its dimension is also  $s_1$ . Next, we cover  $\mathcal{B}$  by finitely many neighborhoods  $V_{m_i}, i \in I$ . We may assume that  $V_{m_i}, i \in I$ ,

are closed balls with radius  $\epsilon > 0$ , while  $P_{m,i}v_{i,1}, \dots, P_{m,i}v_{i,s_i}$  is a basis of  $R(P_{m,i})$ , if  $m$  is in  $W_{m_i} = \{m : |m - m_i| \leq 2\epsilon\}$ . Finally, an explicit formula for  $\varphi_{m,i}$  with  $m$  in  $W_{m_i}$  can be given. For  $|m - m_i| \leq 2\epsilon$ , we set

$$\begin{aligned} \varphi_{m,i} &: K^{s_i} \rightarrow R(P_{m,i}), \\ (a_1, \dots, a_{s_i}) &\mapsto a_1 P_{m,i}v_{1,i} + \dots + a_{s_i} P_{m,i}v_{s_i,i}. \end{aligned}$$

**Lemma 3.1.** *Consider the framework and assumptions in section 2.1. For  $i$  in  $I$ ,  $m$  in  $V_{m_i}$ , and  $q$  in  $\mathbb{R}^p$  with  $|q| = 1$ , the linear function  $(u, v) \mapsto \partial_q(A_m \varphi_{m,i})u + \varphi_{m,i}v$  is injective on  $K^{s_i} \times K^{s_i}$ .*

**Proof:** Assume that  $\partial_q(A_m \varphi_{m,i})u + A_m \varphi_{m,i}v = 0$ , for some  $(u, v)$  in  $K^{s_i} \times K^{s_i}$ . Then

$$(\partial_q A_m) \varphi_{m,i}u + A_m(\partial_q \varphi_{m,i}u + \varphi_{m,i}v) = 0,$$

and using (U2),  $\varphi_{m,i}u = 0$  and  $\partial_q \varphi_{m,i}u + \varphi_{m,i}v = 0$ . As  $\varphi_{m,i}$  is a bijection, this implies that  $u = v = 0$ .  $\square$

**Proposition 3.2.** *Assume that the projectors  $P_{m_i}$ , with  $i \in I$ , are defined as specified above in conjunction with the framework and assumptions in section 2.1. Then there is a positive constant  $C$  such that for all  $m, m'$  in  $\mathcal{B}$ ,*

$$\|A_m u - A_{m'} v\| \geq C(|m - m'| \|v\| + \|u - v\|), \quad (11)$$

for all  $u$  and  $v$  linear combinations of eigenvectors of  $A_m^* A_m$  and  $A_{m'}^* A_{m'}$  where  $m \in V_{m_i}$ ,  $m' \in V_{m_j}$ ,  $u \in R(P_{m,i})$ ,  $v \in R(P_{m,j})$ .

**Proof:** Fix  $i$  in  $I$ . By Proposition 3.1 and Lemma 3.1, using the bijections  $\varphi_{m,i}$ , there is a positive constant  $C_i$  such that for all  $m, m'$  in  $W_{m_i}$ ,  $\tilde{u}, \tilde{v}$  in  $K^{s_i}$ ,

$$\|A_m \varphi_{m,i} \tilde{u} - A_{m'} \varphi_{m',i} \tilde{v}\| \geq C_i(|m - m'| \|\tilde{v}\| + \|\tilde{u} - \tilde{v}\|).$$

Using that  $\varphi_{m,i}$  is a linear bijection from  $K^{s_i}$  to  $R(P_{m,i})$  such that its norm and the norm of its inverse are bounded for  $m$  in  $W_{m_i}$ , re-adjusting  $C_i$  we may write

$$\|A_m P_{m,i} u - A_{m'} P_{m',i} v\| \geq C_i(|m - m'| \|P_{m',i} v\| + \|P_{m,i} u - P_{m',i} v\|), \quad (12)$$

for all  $m, m'$  in  $V_{m_i}$ ,  $u, v$  in  $E$ . It follows that

$$\|A_m P_{m,i} u - A_{m'} P_{m',i} v\| \geq C(|m - m'| \|P_{m',i} v\| + \|P_{m,i} u - P_{m',i} v\|),$$

for all  $u, v$  in  $E$ ,  $i$  in  $I$ , and  $m, m'$  in  $\mathcal{B}$  such that  $|m - m_i| < \epsilon$ ,  $|m' - m_i| < \epsilon$ , with  $C = \min_{i \in I} C_i$ . Next assume, that  $m, m'$  are such that  $|m - m'| < \epsilon$ ,  $m \in V_{m_i}$ ,  $m' \in V_{m_j}$ , and  $i \neq j$ . Then  $R(P_{m,i}) \subset R(P_{m,j})$  or  $R(P_{m,j}) \subset R(P_{m,i})$ . Assume that  $R(P_{m,i}) \subset R(P_{m,j})$ . Then by (12), as  $m$  and  $m'$  are in  $W_{m_j}$ ,

$$\|A_m P_{m,j} u - A_{m'} P_{m',j} v\| \geq C(|m - m'| \|P_{m',j} v\| + \|P_{m,j} u - P_{m',j} v\|).$$



But as  $R(P_{m,i}) \subset R(P_{m,j})$ ,  $P_{m,j}P_{m,i} = P_{m,i}$  thus we find that

$$\|A_m P_{m,i}u - A_{m'} P_{m',j}v\| \geq C(|m - m'| \|P_{m',j}v\| + \|P_{m,i}u - P_{m',j}v\|).$$

The case  $R(P_{m,j}) \subset R(P_{m,i})$  is handled similarly.

There now remains to show that

$$\inf \frac{\|A_m P_{m,i}u - A_{m'} P_{m',j}v\|}{|m - m'| \|P_{m',j}v\| + \|P_{m,i}u - P_{m',j}v\|} > 0, \quad (13)$$

where the inf is taken over the set  $i, j \in I$ ,  $m \in V_i$ ,  $m' \in V_j$ , such that  $|m - m'| \geq \epsilon$  and  $u, v$  in  $E$  such that the denominator  $|m - m'| \|P_{m',j}v\| + \|P_{m,i}u - P_{m',j}v\|$  is positive. If  $P_{m',j}v = 0$  it suffices to show that

$$\inf_{i \in I, u \in V_{m_i}, \|P_{m,i}u\| > 0} \frac{\|A_m P_{m,i}u\|}{\|P_{m,i}u\|} > 0. \quad (14)$$

By (10),  $P_m$  is the orthogonal projection on the sum of eigenspaces corresponding to the eigenvalues of  $A_m^* A_m$  greater than  $\frac{\lambda_N^2(m_i) + \lambda_{N+1}^2(m_i)}{2}$  so the inf in (14) is greater than

$$\min_{i \in I} \left[ \frac{\lambda_N^2(m_i) + \lambda_{N+1}^2(m_i)}{2} \right]^{\frac{1}{2}}.$$

Now, let  $d$  be greater than the diameter of  $\mathcal{B}$ . As  $|m - m'| \|P_{m',j}v\| + \|P_{m,i}u - P_{m',j}v\| \leq (d + 1) \|P_{m',j}v\| + \|P_{m,i}u\|$ , it suffices to show that

$$\inf \frac{\|A_m P_{m,i}u - A_{m'} P_{m',j}v\|}{(d + 1) \|P_{m',j}v\| + \|P_{m,i}u\|} > 0,$$

where the inf is taken over the same set as in the inf in (13). Arguing by contradiction, assume that there are two sequences  $i_n, j_n$  in  $I$ ,  $m_n, m'_n$  in  $B$  with  $m_n \in V_{i_n}$ ,  $m'_n \in V_{j_n}$  such that  $|m_n - m'_n| \geq \epsilon$ , and two sequences  $u_n, v_n$  in  $E$  such that  $\|P_{m'_n, j_n} v_n\| > 0$  and

$$\lim_{n \rightarrow \infty} \frac{\|A_{m_n} P_{m_n, i_n} u_n - A_{m'_n} P_{m'_n, j_n} v_n\|}{(d + 1) \|P_{m'_n, j_n} v_n\| + \|P_{m_n, i_n} u_n\|} = 0.$$

Set  $\omega_n = \frac{\|P_{m_n, i_n} u_n\|}{(d+1) \|P_{m'_n, j_n} v_n\| + \|P_{m_n, i_n} u_n\|}$ . We have

$$\lim_{n \rightarrow \infty} \omega_n A_{m_n} \frac{P_{m_n, i_n} u_n}{\|P_{m_n, i_n} u_n\|} - (1 - \omega_n)(d + 1)^{-1} A_{m'_n, j_n} \frac{P_{m'_n, j_n} v_n}{\|P_{m'_n, j_n} v_n\|} = 0.$$

By compactness after extracting subsequences we can assume that  $i_n \rightarrow i$ ,  $j_n \rightarrow j$  in  $I$ ,  $\omega_n$  converges to  $\omega$  in  $[0, 1]$ ,  $m_n$  converges to  $m$  in  $V_i$ , and  $m'_n$  converges to  $m'$  in  $V_j$ . Necessarily  $|m - m'| \geq \epsilon$ . Note that  $\frac{P_{m_n, i_n} u_n}{\|P_{m_n, i_n} u_n\|} = P_{m_n, i} \frac{P_{m_n, i_n} u_n}{\|P_{m_n, i_n} u_n\|}$ . Since each operator  $P_{m, i}$  is compact and  $m \mapsto P_{m, i}$  is continuous in the closed ball  $V_{m_i}$  of  $\mathbb{R}^p$ , after extracting a subsequence, this converges strongly to some  $\phi$  in  $R(P_{m, i})$  with  $\|\phi\| = 1$ . Similarly,  $\frac{P_{m'_n, j_n} v_n}{\|P_{m'_n, j_n} v_n\|}$  converges strongly to some  $\psi$  in  $R(P_{m', j})$  with  $\|\psi\| = 1$ . At the limit we find

$$\omega A_m \phi - (1 - \omega)(d + 1)^{-1} A_{m'} \psi = 0,$$

contradicting the assumption (P1) if  $0 < \omega < 1$ . If  $\omega = 0$  or  $\omega = 1$ , this contradicts the assumption (U2).  $\square$

In practice, we would like to state a regularity result based on the first singular vectors of  $A_m$ . We now define more precisely what is meant by first singular vectors. Fix a positive integer  $N$ . For  $m$  in  $\mathcal{B}$ , define a subspace  $E_{m,N}$  of  $E$ , with  $\dim E_{m,N} = N$ , such that

$$E_{m,N} \subset \text{Ker} (A_m^* A_m - \lambda_1^2(m)I),$$

or for some integer  $r$ ,

$$\sum_{j=1}^{r-1} \text{Ker} (A_m^* A_m - \lambda_j^2(m)I) \subset E_{m,N} \subset \sum_{j=1}^r \text{Ker} (A_m^* A_m - \lambda_j^2(m)I).$$

**Theorem 3.1.** *Consider the framework and assumption in Subection 2.1. Fix a positive integer  $N$ . Then there is a positive constant  $C$  such that for all  $m, m'$  in  $\mathcal{B}$  and all  $u \in E_{m,N}$  and  $v \in E_{m',N}$ ,*

$$\|A_m u - A_{m'} v\| \geq C(|m - m'| \|v\| + \|u - v\|). \quad (15)$$

**Proof:** Constructing  $V_{m_i}, i \in I$  as in the proof of Proposition 3.2,  $s_i$ , which denoted the dimension of  $R(P_{m_i})$  satisfies  $s_i \geq N$ . It follows that  $E_{m,N} \subset R(P_{m_i})$ , for all  $i \in I$  and  $m$  in  $V_{m_i}$ . Since the sets  $V_{m_i}$  cover  $\mathcal{B}$ , the result is proved.  $\square$

**Remark:** Although the finite-dimensional case was covered by Proposition 3.1, the statement from Theorem 3.1 may be more useful in practice. Indeed, if  $E$  is finite-dimensional, given that our conditions (U1)-(U2) imply that  $A_m^* A_m$  is injective, it is also bijective. However, the norm of  $(A_m^* A_m)^{-1}$  may be very large making this operator impractical to use on  $E$ . Using the spaces  $E_{m,N}$  amounts to reducing  $A_m^* A_m$  to a subspace where this operator is well-conditioned. In the application showed in this paper, we actually obtain satisfactory results with  $N = 5$ .

### 3.3 Application to neural network approximations

Suppose that the conditions for Proposition 3.1 to hold are met. Then  $\mathcal{A}$  defined by (1) has an inverse on  $\mathcal{A}(\mathcal{B} \times E_c)$  which is Lipschitz continuous where,

$$E_c = \{u \in E : \|u\| \geq c\},$$

and  $c$  is a positive constant.

Thus it can be approximated by an NN. Since  $\mathcal{A}^{-1}$  is Lipschitz regular, the growth of the depth of this NN and of the number nodes can be estimated given accuracy requirements. There are by now many papers in the NN literature that provide upper bounds for the size of neural networks approximating Lipschitz functions. For example, we refer to [25, 15] for estimates valid if the ReLU function is used for activation and [5] if the hyperbolic tangent function (tanh) is used instead.

Now suppose that the conditions for Theorem 3.1 to hold are met. Consider  $\mathcal{A} : \mathcal{B} \times E_{m,N,1} \rightarrow F$  where

$$E_{m,N,1} = \{u \in E_{m,N}, \|A_m u\| = 1\}.$$

The condition  $\|A_m u\| = 1$  guarantees that  $u$  is bounded away from zero, uniformly in  $m$  according to the proof of Proposition 3.2. This condition is convenient to impose in practice in an inverse problem by normalizing the measurement  $\|A_m u\|$ . Here too,  $\mathcal{A}$  defined by (1) has an inverse on  $\mathcal{A}(E_{m,N,1})$  which is Lipschitz continuous. Consequently, in this case too, we can approximate  $\mathcal{A}^{-1}$  by a neural network with a control on the upper bounds for the size.

## 4 Discussion and application to an inverse scattering problem

Wave phenomena are ubiquitous. Waves carry information about the environment in which they propagate. This information can be analyzed with forward and inverse modeling. Forward modeling predicts wave behavior, while inverse modeling identifies underlying parameters of interest describing the environment. Recently, NNs leveraging machine learning (ML) techniques have played a pivotal role in improving physics-constrained parameter identification. Ideally, one would want to prove and test the accuracy and robustness of such NNs. Understandably, they depend on the regularity (in this paper, Lipschitz regularity) of the underlying inverse function.

The application to inverse scattering covered in this section is defined on an unbounded domain. This requires the wave function to satisfy a radiation condition (RC) at infinity. The RC is crucial for modeling wave propagation in unbounded domains. Measurable quantities of interest (QOIs), such as scattered fields and far fields, constitute data for the inverse scattering problem. Without an RC, bounded domain PDEs and associated inverse problems have lately been investigated using NN-based solutions. Many references can be found in the survey article [4]. Simply put, the availability of automatic differentiation in open-source NN-optimized frameworks like PyTorch and TensorFlow has facilitated these recent studies. These frameworks symbolically incorporate the underlying PDE in NN loss functions by sampling the PDE in the bounded domain. The survey article [4] highlights the widespread adoption of Physics-Informed Neural Networks (PINNs) for such forward and inverse bounded domain PDEs. Notably, the survey emphasizes (see the last line of its abstract) that fundamental theoretical challenges remain unresolved for PINN-based approaches to both forward and inverse problems, even within the context of bounded-domain PDEs.

Computational methods that preserve the RC without truncating the unbounded region of the PDE often rely on boundary integral representations [3, 14]. In this approach, an equivalent boundary integral equation (BIE) is formed [3]. Integral formulations present the advantage of seamlessly incorporating the RC [3, 14]. These BIEs were mainly developed for wave propagation problems with a constant refractive index [3]. However, by employing domain decompositions as in [7, 8], heterogeneous media can be handled by astute combinations of finite element methods and BIEs.

It is important to point out that NN based solutions to inverse scattering problems differ drastically from non-ML approaches. For instance, we refer to [3] for the classical deterministic Tikhonov regularization approach to inverse scattering problem. This approach requires multiple solves of the forward model to set up the Fréchet derivative for Newton iterations. In contrast, stochastic approximations for constructing posterior distribution of the vector parameter  $m$  can be performed using a Bayesian framework. This framework is robust but also necessitates solving forward models multiple times to establish the likelihood function: see [10] which introduces an online/offline Bayesian method for inverting electromagnetic parameters from noisy far-field data and [10, 23, 19, 18] about the half-space elasticity case. Note that for fast forward model evaluations within a Bayesian framework, an NN surrogate for an exterior Helmholtz model was developed in [9].

We now examine a specific forward model governed by the Helmholtz equation in unbounded regions of  $\mathbb{R}^d$ , where  $d = 2, 3$ . We establish the well-posedness of these models. Next, we focus on the two-dimensional case and describe the parameter  $m$  used to represent crack geometries. We prove that this parameterized model satisfies the two conditions (U1)-(U2), ensuring Lipschitz regularity of the inverse function  $A_m u \mapsto m$ .

#### 4.1 Helmholtz forward models in unbounded regions

Let  $\Gamma$  be a Lipschitz open curve/surface in  $\mathbb{R}^d$ , Let  $D$  be a domain in  $\mathbb{R}^d$  with boundary  $\partial D$  is such that  $\Gamma \subset \partial D$ . The trace theorem (which is also valid in Lipschitz domains [6]), allows us to define an inner and outer trace in  $H^{\frac{1}{2}}(\partial D)$  of functions defined in  $\mathbb{R}^d \setminus \partial D$  with local  $H^1$  regularity. Let  $k$  be in  $L^\infty(\mathbb{R}^d)$  such that

(H1)  $k$  is real-valued;

(H2) there is a positive constant  $k_{min}$  such that  $k \geq k_{min}$  almost everywhere in  $\mathbb{R}^d$ ;

(H3) there exists positive constants  $R_0, k_0$  such that if  $|x| \geq R_0$ , and  $x \in \mathbb{R}^d \setminus \bar{\Gamma}$ ,  $k(x) = k_0$ .

We impose on  $\Gamma$  a Dirichlet condition. Physically, this data could be derived from an incoming incident wave while the problem is solved for a scattered wave. For that kind of problem,  $\Gamma$  is often called a screen. One can find excellent references in the literature for the case where  $k^2$  is constant in space [11, 16, 24]. In particular, these references include an analysis of singularities of the solution at the tip of the crack and the analysis of numerical methods for solving these problems using integral equations on  $\Gamma$ .

In this work, we consider the Dirichlet crack forward scattering problem to be the unbounded-region boundary value problem (BVP) with Sommerfeld RC: Find  $u \in \mathcal{V}$  such that

$$(\Delta + k^2)u = 0 \text{ in } \mathbb{R}^d \setminus \bar{\Gamma}, \quad (16)$$

$$u = g \text{ on } \Gamma, \quad (17)$$

$$\frac{\partial u}{\partial r} - ik_0 u = O(|x|^{-(d+1)/2}), \text{ as } r \rightarrow \infty, \quad (18)$$

where  $g$  is the restriction to  $\Gamma$  of a function in  $H^{\frac{1}{2}}(\partial D)$ , and  $\mathcal{V}$  is a function space on which the BVP with the RC in (18) is well posed and that the solution  $u$  depends continuously on

$g$ . Following [14, Section 2.6] we define  $\mathcal{V}$  defined, first for  $d = 2$ , as

$$\mathcal{V} = \left\{ v \in H_{loc}^1(\mathbb{R}^2 \setminus \bar{\Gamma}) : \frac{v}{\sqrt{1 + |x| \ln(2 + |x|)}}, \frac{\nabla v}{\sqrt{1 + |x| \ln(2 + |x|)}}, \frac{\partial v}{\partial r} - ik_0 v \in L^2(\mathbb{R}^2 \setminus \bar{\Gamma}) \right\},$$

and then for  $d = 3$  as

$$\mathcal{V} = \left\{ v \in H_{loc}^1(\mathbb{R}^3 \setminus \bar{\Gamma}) : \frac{v}{\sqrt{1 + |x|^2}}, \frac{\nabla v}{\sqrt{1 + |x|^2}}, \frac{\partial v}{\partial r} - ik_0 v \in L^2(\mathbb{R}^3 \setminus \bar{\Gamma}) \right\}.$$

In applications,  $g$  is commonly set equal to minus the value of an incoming incident field and  $u$  represents the scattered field for a problem while the total field is zero on  $\Gamma$ .

**Proposition 4.1.** *The BVP (16-18) is uniquely solvable. The solution  $u$  in  $\mathcal{V}$  depends continuously on the forcing term  $g$  in  $H^{\frac{1}{2}}(\Gamma)$ .*

**Proof:** We first show uniqueness. Assume that  $g = 0$ . Let  $S_R$  be the sphere centered at the origin with radius  $R$ . Applying Green's theorem we find that  $\text{Im} \int_{S_R} u \frac{\partial \bar{u}}{\partial r} = 0$ . Next, since  $u \in \mathcal{V}$ , there is a sequence  $R_n \rightarrow \infty$  such that,

$$\lim_{n \rightarrow \infty} \int_{S_{R_n}} \left| \frac{\partial u}{\partial r} - ik_0 u \right|^2 = 0,$$

so altogether we have that,

$$\lim_{n \rightarrow \infty} \int_{S_{R_n}} \left| \frac{\partial u}{\partial r} \right|^2 + |u|^2 = 0.$$

Due to Rellich's lemma for far field patterns, it follows that  $u(x) = 0$ , if  $|x| > R_0$ . Since the only regularity assumption on  $k$  is that it is in  $L^\infty$  there is no elementary argument for showing that  $u(x)$  is zero if  $|x| \leq R_0$ . However, we can use results from the unique continuation literature, in particular, the corollary of Theorem 1 in [1] to claim that  $u$  is zero throughout  $\mathbb{R}^d \setminus \bar{\Gamma}$ .

Next, we show existence. Fix  $R' > R_0$ . Let  $B_{R'}$  the open ball centered at the origin of  $\mathbb{R}^d$  with radius  $R'$ . We can extend  $g$  to a function  $\psi$  in  $H^1(\mathbb{R}^d)$  supported strictly inside  $B_{R'}$ . Using a continuous extension operator,  $\psi$  depends continuously on  $g$ . We now seek to solve an equivalent problem for  $\tilde{u} = u - \psi$ . Define the closed subspace  $H_{\Gamma,0}^1(B_{R'})$  of  $H^1(B_{R'})$ ,

$$H_{\Gamma,0}^1(B_{R'}) = \{w \in H^1(B_{R'}) : v = 0 \text{ on } \Gamma\}.$$

Note that this definition requires the trace of  $v$  on  $\Gamma$  to be zero on each side. Define the bilinear functional,

$$b(v, w) = \int_{B_{R'}} \nabla v \cdot \nabla w - k^2 v w - \int_{S_{R'}} T_{R',k_0} v w, \quad (19)$$

for  $v, w \in H^1(B_{R'})$  and where  $T_{R',k_0}$  is the Dirichlet to Neumann map for radiating solutions to the Helmholtz equation in the exterior of  $B_{R'}$  with wavenumber  $k_0$ .  $T_{R',k_0}$  is known to

be a continuous mapping from  $H^{\frac{1}{2}}(S_{R'})$  to  $H^{-\frac{1}{2}}(S_{R'})$ , while  $-T_{R',0}$  is strictly coercive, and  $T_{R',k_0} - T_{R',0}$  is compact from  $H^{\frac{1}{2}}(S_{R'})$  to  $H^{-\frac{1}{2}}(S_{R'})$ , see [3, Section 5.2] or [14, Section 2.6.5]. According to the uniqueness property covered above, we have that if  $v \in H^1(B_{R'})$  and  $B(v, w) = 0$  for all  $w \in H^1(B_{R'})$ , then  $v = 0$ .

Now, consider the variational problem:

$$\begin{aligned} \text{find } \tilde{u} \in H_{\Gamma,0}^1(B_{R'}) \text{ such that } \forall w \in H_{\Gamma,0}^1(B_{R'}), \\ \mathfrak{b}(\tilde{u}, w) = -\mathfrak{b}(\psi, w). \end{aligned} \quad (20)$$

This problem has at most one solution since  $\mathfrak{b}$  is non-degenerate. Existence follows by arguing that this problem is in the form strictly coercive plus compact, which is the case thanks to the properties of the operator  $T_{R',k_0}$  recalled above. Finally,  $u = \tilde{u} + \psi$  can be extended to  $\mathbb{R}^d \setminus \bar{\Gamma}$  as a function satisfying (16-18).  $\square$

If  $k^2$  is constant in  $\mathbb{R}^d$  the solution  $u$  to the BVP (16-18) can be written in integral form.

$$u(x) = \int_{\Gamma} \Phi(x, y) \left[ \frac{\partial u}{\partial n}(y) \right] d\sigma(y), \quad (21)$$

with  $\Phi$  the free space Green function for the Helmholtz equation and  $\left[ \frac{\partial u}{\partial n} \right]$ , the jump of  $\frac{\partial u}{\partial n}$  across  $\Gamma$ , is in  $H^{-\frac{1}{2}}(\Gamma)$ , see [17]. Referring to the BVP (16-18), suppose that  $\left[ \frac{\partial u}{\partial n} \right]$  is zero on  $\Gamma \cap B$ , where  $B$  is an open ball with center on  $\Gamma$ . Then  $u$  is locally  $H^1$  in  $B$  and satisfies  $(\Delta + k^2)u = 0$  in  $B$ . Then  $B$  can be taken out from  $\Gamma$  without changing the solution  $u$ . We thus make the following minimal assumption on  $\Gamma$ :

$$(J1) \quad \left[ \frac{\partial u}{\partial n} \right] \text{ has full support in } \Gamma,$$

or equivalently,

$$(J2) \quad \text{for any open ball } B \text{ centered on } \Gamma, u \text{ cannot be extended to a function satisfying } (\Delta + k^2)u = 0 \text{ in } B.$$

**Theorem 4.1.** *For  $i = 1, 2$ , let  $\Gamma_i$  be a Lipschitz open surface, let  $u^i$  be the unique solution to the BVP (16-18) with  $\Gamma_i$  in place of  $\Gamma$  and the Dirichlet condition  $g^i$  in  $H^{1/2}(\Gamma_i)$  in place of  $g$ . Let  $R$  be greater or equal than  $R_0$ . Let  $S_R$  be a sphere. Assume that  $\mathbb{R}^d \setminus \overline{\Gamma_1 \cup \Gamma_2}$  is connected and that  $g^i$  has full support in  $\overline{\Gamma_i}$ ,  $i = 1, 2$ . If  $u^1 = u^2$  on  $S_R$ , then  $\overline{\Gamma_1} = \overline{\Gamma_2}$  and  $g^1 = g^2$  almost everywhere.*

**Proof:** Set  $U = \mathbb{R}^d \setminus \overline{\Gamma_1 \cup \Gamma_2}$ ,  $u = u^1 - u^2$  in  $U$ . We can then argue as in the proof of Proposition 4.1 that  $u$  is zero in  $U$ . Next, we argue by contradiction: suppose that there is an  $x$  in  $\Gamma_1$  such that  $x \notin \overline{\Gamma_2}$ . Then there is an open ball  $B(x, r)$  centered at  $x$  with radius  $r > 0$  such that  $B(x, r) \cap \overline{\Gamma_2} = \emptyset$ . Now  $\left[ \frac{\partial u}{\partial n} \right] = 0$  on  $B(x, r) \cap \overline{\Gamma_1}$ , and as  $(\Delta + k^2)u^2 = 0$  in  $B(x, r)$ ,  $\left[ \frac{\partial u^2}{\partial n} \right] = 0$  on  $B(x, r) \cap \overline{\Gamma_1}$ . It follows that  $\left[ \frac{\partial u^1}{\partial n} \right] = 0$  on  $B(x, r) \cap \overline{\Gamma_1}$ , contradicting (J1). We conclude that  $\Gamma_1 \subset \overline{\Gamma_2}$ . Reversing the roles of  $\Gamma_1$  and  $\Gamma_2$  we then find that  $\overline{\Gamma_1} = \overline{\Gamma_2}$ . Using one more time that  $u$  is zero in  $U$ , since  $u = 0$  on each side of  $\Gamma_1 = \Gamma_2$ , it follows that  $g_1 - g_2 = 0$  almost everywhere in  $\Gamma_1$ .  $\square$

## 4.2 Crack inverse problem: verifying conditions (U1)-(U2)

We start from the solution  $u$  to the BVP (16-18) written in integral form (21) for the case  $d = 2$  with a concrete parametric description of a linear crack  $\Gamma$ . For this case, the kernel in (21) is given by

$$\Phi(x, y) = \frac{i}{4} \mathcal{H}_0^1(k|x - y|). \quad (22)$$

The line supporting the linear crack  $\Gamma$  can be parametrized by choosing a unit vector direction  $\tau$  and an offset scalar parameter  $a$  such that this line goes through the point  $an \in \mathbb{R}^2$ , with  $n$  an outward unit vector normal to  $\Gamma$  at the point. The solution  $u$  to problem (16-18) can then be written in integral form as

$$u(x) = \int_{-M}^M \Phi(x, y(t)) \left[ \frac{\partial u}{\partial n} \right] (y(t)) dt, \quad (23)$$

$$y(t) = \tau t + an, \quad (24)$$

$$\tau = (\cos \theta, \sin \theta), \quad n = (-\sin \theta, \cos \theta), \quad (25)$$

where  $M$  is such that the support of  $\left[ \frac{\partial u}{\partial n} \right] (y)$  is in  $[-M, M]$  with  $y = \tau t + an$ .

Accordingly, with vector parameter  $m = (\theta, a)$ , we define a concrete application based form of the parameterized forward model operator  $A_m$  discussed in the first three section of this article, using the framework in section 2.1 with  $K = \mathbb{C}$ ,  $E = H^{-\frac{1}{2}}((-M, M))$ ,  $F = L^2(S_R)$ , and

$$\mathcal{B} = \{(\theta, a) : \theta \in [-\pi/2, \pi/2], -a_{\max} \leq a \leq a_{\max}\} \subset \mathbb{R}^2, \quad (26)$$

where

(B1) the constants  $R, M, a_{\max}$  are such that the distance from the line segment  $t\tau + an$ ,  $-M \leq t \leq M$ , to the circle  $S_R$  is bounded by a positive constant.

The interval  $[-\pi/2, \pi/2)$  is compact for the circular metric

$$\delta(\theta, \theta') = \sqrt{(\cos 2\theta - \cos 2\theta')^2 + (\sin 2\theta - \sin 2\theta')^2}.$$

In (26),  $\theta$  is restricted to  $[-\pi/2, \pi/2)$  because the associated parametrized compact operator  $A_m$ , defined below, is invariant as  $(\theta, a, t)$  is changed to  $(\theta + \pi, -a, -t)$ . In particular, we are interested in the inversion of the operator  $A_m : H^{-\frac{1}{2}}((-M, M)) \rightarrow L^2(S_R)$ , induced by the solution in (23):

$$A_m \psi = u|_{S_R}, \quad \text{where } u(x) = \int_{-M}^M \Phi(x, y(t)) \psi(t) dt. \quad (27)$$

It is clear due to formulation (23) that  $A_m$  is  $C^1$  in  $m = (\theta, a)$ .

Thus if we prove that conditions (U1)-(U2) are satisfied by the concrete operator (27), we can claim the Lipschitz regularity of the inverse of the operator. The rest of this section is on proving these two assumptions to facilitate solving the inverse parameter model for the crack using NN approximations in the next section.

First we prove the injective of the operator in  $A_m$  in (27).

**Lemma 4.1.** [Condition (U1) holds] For all  $\psi, \phi$  in  $H^{-\frac{1}{2}}((-M, M))$ , for all  $m, m'$  in  $\mathcal{B}$ , if  $\psi \neq 0$ ,  $A_m\psi = A_{m'}\phi$  implies  $m = m'$  and  $\psi = \phi$ .

**Proof:** We set  $u^1(x) = \int_{-M}^M \Phi(x, y)\psi(t)dt$ ,  $u^2(x) = \int_{-M}^M \Phi(x, y)\phi(t)dt$ , with  $y$  as in (24). Then by Theorem 4.1,  $m = m'$  and  $u^1 = u^2$  outside the line defined by (24). It follows that the jump of the normal derivative of  $u^1$  across that line equals the jump of the normal derivative of  $u^2$  so  $\psi = \phi$ .  $\square$

As previously,  $\partial_q A_m$  denotes a partial derivative of  $A_m$  with respect to the parameter  $m$  in the direction of  $q$ .

**Proposition 4.2.**  $\partial_q A_m$  is injective on  $H^{-\frac{1}{2}}((-M, M))$ , for all  $q$  in  $\mathbb{R}^2$  with  $|q| = 1$ , and  $m$  in  $\mathcal{B}$ , defined (26).

**Proof:** Assume that  $\partial_q A_m\psi = 0$  for some  $\psi$  in  $H^{-\frac{1}{2}}((-M, M))$ , and  $q = (q_1, q_2)$ ,  $|q| = 1$ . Since  $m = (\theta, a)$ , using (24),  $\frac{\partial y}{\partial \theta} = nt - a\tau$ , and  $\frac{\partial y}{\partial a} = n$ . According to the chain rule, for all  $x$  in  $S_R$ ,

$$\begin{aligned} \partial_q A_m\psi &= q_1 \frac{\partial}{\partial \theta} A_m\psi + q_2 \frac{\partial}{\partial a} A_m\psi \\ &= q_1 \int_{-M}^M \nabla_y \Phi(x, y) \cdot (nt - a\tau)\psi(t)dt + q_2 \int_{-M}^M \nabla_y \Phi(x, y) \cdot n\psi(t)dt. \end{aligned}$$

Define  $w(x)$  by the formula in the previous line for all  $x$  in  $\mathbb{R}^2 \setminus \bar{\Gamma}$ . By construction,  $w(x) = 0$  for all  $x$  on  $S_R$ , and  $(\Delta + k^2)w = 0$  in  $\mathbb{R}^2 \setminus \bar{\Gamma}$ . Since  $\frac{w}{\sqrt{1+r^2 \ln(2+r)}}$ ,  $\frac{\nabla w}{\sqrt{1+r^2 \ln(2+r)}}$ ,  $\frac{\partial w}{\partial r} - ikw \in L^2(\mathbb{R}^2 \setminus \bar{\Gamma})$ , it follows that  $w$  is zero in  $\mathbb{R}^2 \setminus \bar{\Gamma}$ . The jump of  $w$  across  $\Gamma$  can be determined according to the rules shown in [22, Lemma 1] or [22, Appendix C]. According to these jump formulas we find that  $(q_1 t + q_2)\psi(t) = 0$  inside the support of  $\psi$ . As  $|q| = 1$ , it follows that  $g = 0$ .  $\square$

**Proposition 4.3.** [Condition (U2) holds] Let  $\psi, \phi$  be in  $H^{-\frac{1}{2}}((-M, M))$ , and  $q \in \mathbb{R}^2$  be a unit vector. If  $\partial_q A_m\psi = A_m\phi$  then  $\psi = \phi = 0$ .

**Proof:** Assume that  $\partial_q A_m\psi - A_m\phi = 0$  for some  $\psi, \phi$  in  $H^{-\frac{1}{2}}((-M, M))$ , and  $q = (q_1, q_2)$ ,  $|q| = 1$ . According to the chain rule, for all  $x$  in  $S_R$ ,

$$\begin{aligned} &\partial_q A_m\psi - A_m\phi \\ &= q_1 \frac{\partial}{\partial \theta} A_m\psi + q_2 \frac{\partial}{\partial a} A_m\psi - A_m\phi \\ &= q_1 \int_{-M}^M \nabla_y \Phi(x, y) \cdot (nt - a\tau)\psi(t)dt + q_2 \int_{-M}^M \nabla_y \Phi(x, y) \cdot n\psi(t)dt - \int_{-M}^M \Phi(x, y)\phi(t)dt. \end{aligned}$$

Define  $w(x)$  by the formula in the previous line for all  $x$  in  $\mathbb{R}^2 \setminus \bar{\Gamma}$ . Just as in the proof of Proposition 4.2 we can argue that  $w$  is zero in  $\mathbb{R}^2 \setminus \bar{\Gamma}$ . Now, the term  $\int_{-M}^M \Phi(x, y)\phi(t)dt$  is known to be continuous across  $\Gamma$ . Thus, just as in the proof of Proposition 4.2 we find that  $(q_1 t + q_2)\psi(t) = 0$  inside the support of  $\psi$ , so  $\psi = 0$ . At this stage, we just need to notice



that since  $\psi = 0$ , the jump of the normal derivative of  $w$  across  $\Gamma$  is  $\phi$ , so  $\phi = 0$ .  $\square$

In summary, we have shown that in the case of a two-dimensional homogeneous scattering medium with a linear crack and Dirichlet conditions on that crack, all requirements for applying Proposition 3.2 are satisfied with  $E = H^{-\frac{1}{2}}((-M, M))$ ,  $F = L^2(S_R)$ , and  $A_m$  defined by (27) if the crack is strictly included in the ball with radius  $R$  as expressed by condition (B1).

Next, as we seek to apply Theorem 3.1, the finite number  $N$  of distinct singular values to be used to construct the projectors  $P_m$  can be arbitrary, but as  $N$  grows large the constant  $C$  in (15) tends to zero. In fact,  $C = O(\tau^{-N})$  for some  $\tau$  in  $(0, 1)$ . This is due to the fact that  $\Phi(x, y)$  is analytic in  $y$  if  $y$  is in some open neighborhood of all possible line segments  $t\tau + an$  such that condition (B1) holds. The exponential decay  $C = O(\tau^{-N})$  was proved in [2, 20].

## 5 Numerical simulations

In this section, we conduct simulations in relation to the inverse problem studied in section 4.2. The goal is to recover the parameter  $m$  in  $\mathcal{B}$  from the data  $A_m\psi$  defined in (27) using an NN. The simulations comprise three stages. First, data for training the NN is built up and stored. Second, the NN is trained on that data. Third, the accuracy and the computational speed of the NN is tested on entirely new data produced by incoming waves, point sources, or arbitrary forcing terms altogether.

### 5.1 Specific values of parameters and bounds

For the the range in the parameter set  $\mathcal{B}$  defined in, (26) we fix  $a_{\max} = 1$ . In our simulations, the constant wavenumber  $k$  is 1.5 and  $R$ , the radius of  $S_R$ , is 4. Next we set bounds for the support of  $\psi$  for condition (B1) to hold. Recalling the  $y$  dependency on  $t$  (24), we require the support of  $\psi$  with regard to  $t$  in (27) to be such that  $t$  is in the interval with center  $o$  in  $[-1, 1]$  and length  $l$  in  $[1, 3]$ . With these numbers the distance from the support of  $\psi$  to  $S_R$  is bounded below by  $\sim 1.3$ .

### 5.2 Discrete approximation of $A_m$ and learning data setup

Recall that  $A_m\psi = \int_{-M}^M \Phi(x, y)\psi(t)dt$  where  $x$  is in  $S_R$  and  $t$  is such that  $y$  is in the support of  $\psi$ . As  $x$  remains bounded from  $y$ ,  $\Phi(x, y)$  is smooth. We then approximate the smooth function  $A_m\psi$  on  $S_R$ , by the vector in  $\mathbb{C}^{N_S}$   $A_m\psi(x_i)$ , with  $x_i = \left(R \cos(j \frac{2\pi}{N_S}), R \sin(i \frac{2\pi}{N_S})\right)$ ,  $i = 1, \dots, N_S$ . There are the scattered field observation points. In our numerical solutions, we used the value  $N_S = 40$ .

The integral  $\int_{-M}^M \Phi(x, y)\psi(t)dt$  equals  $\int_{M_1}^{M_2} \Phi(x, y)\psi(t)dt$  where  $M_1 = o - l/2$ ,  $M_2 = o + l/2$  given the support of  $\psi$ . We then set  $t = \frac{M_2 - M_1}{2}s + \frac{M_2 + M_1}{2}$ ,  $-1 \leq s \leq 1$  to obtain the integral  $\int_{-1}^1 \Phi(x, y)\psi(t) \frac{M_2 - M_1}{2} ds$ . The well-known singularity of  $\psi$  at each endpoint of its

support [17] allows us to write  $\psi(t) = \tilde{\psi}(s)/\sqrt{1-s^2}$ , where  $\tilde{\psi}$  is smooth. This motivates the change of variables  $s = \sin v$ . The integral is then approximated by a finite sum using  $N_\Gamma = 10$  quadrature points for  $v$  forming a uniform grid of  $[-\pi/2, \pi/2]$ . We denote the associated values for  $y, y(v_j), v_j = -\frac{\pi}{2} + (j-1)\frac{\pi}{N_\Gamma-1}$   $j = 1, \dots, N_\Gamma$ . Note that  $y(v_j)$  depends on  $o, l$ , and  $m$ . Altogether,  $A_m$  is approximated by a  $N_S \times N_\Gamma$  complex matrix  $A_{m,app}$  with entries

$$\tau_j \Phi(x_i, y(v_j)) \frac{M_2 - M_1}{2} \frac{\pi}{N_\Gamma - 1}, \quad i = 1, \dots, N_S, \quad j = 1, \dots, N_\Gamma.$$

Here the weights  $\tau_1 = \tau_{N_\Gamma} = \frac{1}{2}$  and  $\tau_j = 1$ , for  $1 < j < N_\Gamma$ , come from the trapezoidal rule, and the constant term  $\frac{M_2 - M_1}{2} \frac{\pi}{N_\Gamma - 1}$  has been omitted since we are only interested in computing singular vectors. The bridge between application of Theorem 3.1 to  $A_{m,app}$  instead of  $A_m$  is covered in [21, Theorem 4.2], which asserts that estimate (15) applies to  $A_{m,app}$  as well with  $C/2$  in place of  $C$ , as long as the dimension  $N_S$  is sufficiently large enough. In fact, this theorem implies that any numerical method based on convergent quadratures could be used for approximating  $A_{m,app}$  from  $A_m$ .

The steps to produce learning data are then:

1. A random geometry is picked for  $\Gamma$ . This is done by picking random values for  $a, \theta$  using uniform probability distributions within their range.
2. A random support is chosen for  $\psi$ . This is done by picking random values for  $o, l$  using uniform probability distributions within their range.
3. For these choices, the matrix  $A_{m,app}$  is set up as described above using (22), the fundamental solution of the Helmholtz equation.
4. The first  $N = 5$  singular values of  $A_{m,app}$  are computed together with corresponding singular vectors  $v_1, \dots, v_5$  in  $\mathbb{C}^{N_S}$ .
5. A random vector  $r_1, \dots, r_5$  is picked in the ball of  $\mathbb{C}^5$  centered at the origin and with radius 1.
6. Let  $w = r_1 v_1 + \dots + r_5 v_5$ . The input for learning is the normalized vector  $w/\|w\|$  and the target is  $(a, \theta)$ .

The set of learning data in our NN simulations comprised  $10^6$  input-target pairs.

### 5.3 Neural network training step

We trained a neural network  $\mathcal{N}$  on this data set.  $\mathcal{N}$  was composed of an entry layer with width 80, three hidden layers with width 80, and one exit layer with width 2. The activation function connecting these layers was chosen to be the hyperbolic tangent function. This architecture, albeit heavy, proved to be adequate for the size of our problem: the inputs are in  $\mathbb{R}^{80}$ , the targets in  $\mathbb{R}^2$ . The inputs actually depend on  $w$  in  $\mathbb{C}^5 \sim \mathbb{R}^{10}$ ,  $(a, \theta)$  in  $\mathbb{R}^2$ , and  $(o, l)$  in  $\mathbb{R}^2$ .

The training was performed using the ADAM algorithm [13]. We found that this stochastic minimization algorithm is particularly efficient given the size of our problem: this algorithm made it possible to compute gradients of the penalty function on randomized mini-batches. Recall that the equation (27) is invariant as  $(\theta, a, t)$  is changed to  $(\theta + \pi, -a, -t)$ . To ensure uniqueness,  $\theta$  was restricted to  $[-\pi/2, \pi/2)$  in (26). However, numerically, there is little difference between the data for  $\theta = -\pi/2, a, \psi(t)$  and  $\theta = \pi/2 - \epsilon, -a, \psi(-t)$  if  $\epsilon > 0$  is small. In practice, we circumvented this difficulty, by computing three neural networks:  $\mathcal{N}_1$  for which  $-\pi/2 \leq \theta < \pi/2$ ,  $\mathcal{N}_2$  for which  $-\pi/2 \leq \theta < 0$ , and  $\mathcal{N}_3$  for which  $0 \leq \theta < \pi/2$ .  $\mathcal{N}_1$  only learns  $\theta$ . If  $\theta$  is determined to be negative by applying  $\mathcal{N}_1$ , then  $\mathcal{N}_2$  is used, otherwise  $\mathcal{N}_3$  is used. This quasi-periodicity issue could instead be resolved by altering the penalty function, at the cost of slowing down the learning process.

## 5.4 Testing the learned neural network

We considered four cases:

- Case 1* The Dirichlet data  $g$  in (17) is the incoming plane wave  $e^{ikx \cdot \eta}$ , where  $\eta$  is a unit vector in  $\mathbb{R}^2$ .
- Case 2* The Dirichlet data  $g$  in (17) is source point wave  $\frac{i}{4}\mathcal{H}_0^1(k|x-s|)$  where  $s$  in  $\mathbb{R}^2$  is such that  $3 \leq |s| \leq 3.5$ . Accordingly the source is between the screen and  $S_R$ .
- Case 3* The Dirichlet data  $g$  in (17) is source point wave  $\frac{i}{4}\mathcal{H}_0^1(k|x-s|)$  where  $s$  in  $\mathbb{R}^2$  is such that  $5 \leq |s| \leq 7$ . Accordingly the source is outside  $S_R$ .
- Case 4* This last case does not use Dirichlet problem (16-18). Instead, the data  $A_m\psi = u|_{S_R}$  is directly formed from a given forcing term.

Two examples of configurations for the fault  $\Gamma$  relative to the circle  $S_R$  are plotted in Figure 1. The left plot corresponds to case 1. This is not a plot of the scattered field  $u$  solution to (16-18). Instead, we plotted the real part of the total field  $u + e^{ikx \cdot \eta}$  which is more easily physically interpreted. The right plot corresponds to case 3. The scale is different for visualization purposes as the total field quickly decays from the source in case 3.

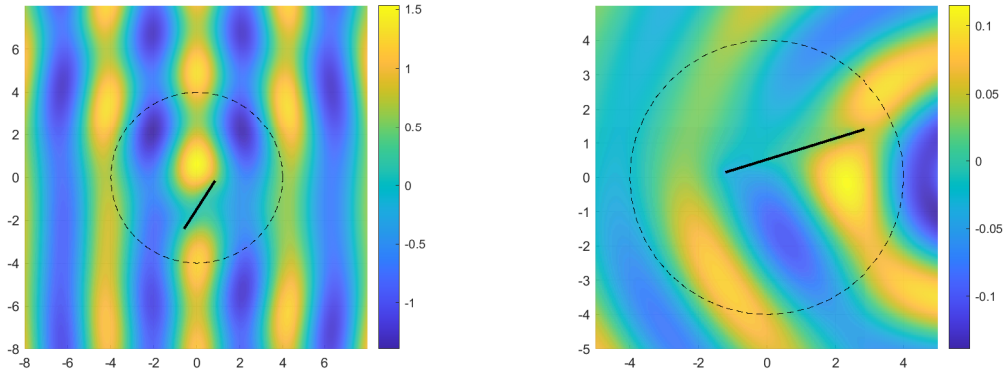


Figure 1: Examples of configurations for the fault  $\Gamma$  relative to the circle  $S_R$  in Figure 1. The real part of the total field is sketched. In each case, the crack  $\Gamma$  is the black line segment. The circle  $S_R$  is the dotted circle. The left plot corresponds to case 1 with incidence angle  $\eta = (1, 0)$ . The right plot corresponds to case 3 with source  $s = (6, 0)$ . The scale is different in order to facilitate visualization as the total field quickly decays from the source.

In Figure 2 we plot absolute errors for computing  $\sin \theta$  and  $a$  using networks  $\mathcal{N}_1, \mathcal{N}_2, \mathcal{N}_3$ . The errors are shown for 1000 randomly generated examples. In each example, a random geometry is picked for  $\Gamma$  by sampling random values for  $a, \theta$  and a random support is chosen for  $\psi$  by sampling random values for  $o, \ell$  (with uniform distributions for  $a, \theta, o, \ell$  within their range). We then randomly switch to case 1, 2, 3, or 4 (with probability 0.25 for each case). In case 1, the incidence angle for  $\eta$  is randomly chosen (with a uniform distribution in  $[0, 2\pi]$ ). In case 2 or 3, the source is randomly chosen, with uniform distribution within its range. In case 4, we pick  $\psi(t) = y_1(t) - i \cos y_2(t)$  where again  $y$  depends on  $t$  through equation (24). We then apply the neural networks  $\mathcal{N}_1$ , then  $\mathcal{N}_2$  or  $\mathcal{N}_3$  to these 1000 cases. Collective run time for these 1000 cases is 0.06 seconds. Absolute errors for  $\sin \theta$  and  $a$  are shown in Figure 2 in blue. The average error for these 1000 cases is about 0.02 for  $\sin \theta$  and 0.03 for  $a$ .

## 5.5 Numerical stability to noise

To simulate the effect of noise, a random perturbation was added to the data for these 1000 trials. For each trial and each coordinate of the data vector in  $\mathbb{R}^{2N_S}$ , we drew a random number in  $[-0.2, 0.2]$  which we then multiplied by the overall sup norm of the data and used the result as additive noise. We show in Figure 3 an example of data  $A_m \psi(R \cos(j \frac{2\pi}{N_S}), R \sin(j \frac{2\pi}{N_S}))$ ,  $j = 1, \dots, N_S$ , for a particular trial. We plotted the real part and the imaginary part of the noise-free data. Noisy data is superimposed. In Figure 2, in red, we show absolute errors on  $\sin \theta$  and  $a$  evaluated applying  $\mathcal{N}_1, \mathcal{N}_2, \mathcal{N}_3$  to the noisy data. The average error for these 1000 trials is about 0.08 for  $\sin \theta$  and 0.09 for  $a$ .

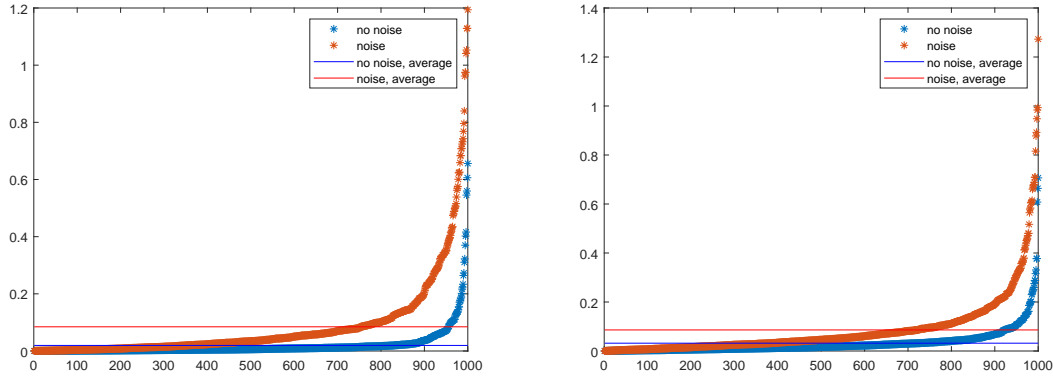


Figure 2: Sorted absolute value errors in evaluating  $\sin \theta$  (left) and  $a$  (right) for 1000 random trials of  $\theta, a$  support of the forcing term  $g$  and random choice of case 1, 2, 3, or 4. The horizontal solid lines indicate average error for the 1000 trials. Blue: noise-free data. Red: noisy data.

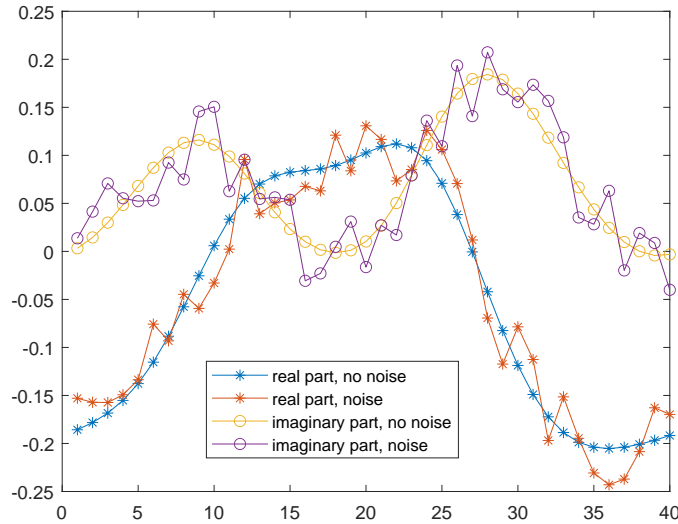


Figure 3: Example of data in  $\mathbb{C}^{N_S}$ . Real and imaginary parts of  $A_m \psi$  at  $(R \cos(j \frac{2\pi}{N_S}), R \sin(j \frac{2\pi}{N_S}))$ ,  $j = 1, \dots, N_S$  are plotted with  $j \frac{2\pi}{N_S}$  on the horizontal axis. The smooth curves correspond to noise-free data. The jagged curves correspond to noisy data.

## References

- [1] B. Barcelo, C. E. Kenig, A. Ruiz, and C. Sogge. Weighted Sobolev inequalities and unique continuation for the laplacian plus lower order terms. *Illinois Journal of Mathematics*, 32(2):230–245, 1988.

- [2] M. S. Birman and M. Z. Solomyak. Estimates of singular numbers of integral operators. *Russian Mathematical Surveys*, 32(1):15, 1977.
- [3] D. L. Colton, R. Kress, and R. Kress. *Inverse acoustic and electromagnetic scattering theory*, volume 93. Springer, 2013.
- [4] S. Cuomo, V. D. Cola, F. Giampaolo, G. Rozza, M. Raissi, and F. Piccialli. Scientific machine learning through physics-informed neural networks: Where we are and what's next. *J. Scientific Computing*, 92:88 (62 pages), 2022.
- [5] T. De Ryck, S. Lanthaler, and S. Mishra. On the approximation of functions by tanh neural networks. *Neural Networks*, 143:732–750, 2021.
- [6] Z. Ding. A proof of the trace theorem of Sobolev spaces on Lipschitz domains. *Proceedings of the American Mathematical Society*, 124(2):591–600, 1996.
- [7] V. Domínguez and M. Ganesh. Analysis and application of an overlapped FEM-BEM for wave propagation in unbounded and heterogeneous media. *Appl. Numer. Math.*, 171:76–105, 2022.
- [8] V. Domínguez, M. Ganesh, and F. J. Sayas. An overlapping decomposition framework for wave propagation in heterogeneous and unbounded media: formulation, analysis, algorithm, and simulation. *J. Comput. Phys.*, 403:109052, 20, 2020.
- [9] M. Ganesh, S. C. Hawkins, N. Kordzakhia, and S. Unicom. An efficient Bayesian neural network surrogate algorithm for shape detection. *ANZIAM J.*, 62:C112–C127, 2022.
- [10] M. Ganesh, S. C. Hawkins, and D. Volkov. An efficient algorithm for a class of stochastic forward and inverse Maxwell models in  $\mathbb{R}^3$ . *J. Comput. Phys.*, 398:10881, 2019.
- [11] G. C. Hsiao, E. P. Stephan, and W. L. Wendland. On the Dirichlet problem in elasticity for a domain exterior to an arc. *Journal of computational and applied mathematics*, 34(1):1–19, 1991.
- [12] T. Kato. *Perturbation theory for linear operators*, volume 132. Springer Science & Business Media, 2013.
- [13] D. P. Kingma. Adam: A method for stochastic optimization. *arXiv preprint arXiv:1412.6980*, 2014.
- [14] J.-C. Nédélec. *Acoustic and electromagnetic equations: integral representations for harmonic problems*, volume 144. Springer, 2001.
- [15] Z. Shen, H. Yang, and S. Zhang. Neural network approximation: Three hidden layers are enough. *Neural Networks*, 141:160–173, 2021.
- [16] E. Stephan and W. L. Wendland. An augmented Galerkin procedure for the boundary integral method applied to mixed boundary value problems. *Applied Numerical Mathematics*, 1(2):121–143, 1985.

- [17] E. P. Stephan and W. L. Wendland. An augmented galerkin procedure for the boundary integral method applied to two-dimensional screen and crack problems. *Applicable Analysis*, 18(3):183–219, 1984.
- [18] D. Volkov. A parallel sampling algorithm for some nonlinear inverse problems. *IMA Journal of Applied Mathematics*, 87(2):187–206, 2022.
- [19] D. Volkov. A stochastic algorithm for fault inverse problems in elastic half space with proof of convergence. *Journal of Computational Mathematics*, 40(6):957–978, 2022.
- [20] D. Volkov. Optimal decay rates in Sobolev norms for singular values of integral operators. *Journal of Mathematical Analysis and Applications*, 537(2):128403, 2024.
- [21] D. Volkov. Stability properties for a class of inverse problems. *Journal of Inverse and Ill-posed Problems*, 32(3):333–350, 2024.
- [22] D. Volkov and Y. Jiang. Stability properties of a crack inverse problem in half space. *Mathematical methods in the applied sciences*, 44(14):11498–11513, 2021.
- [23] D. Volkov and J. C. Sandiumenge. A stochastic approach to reconstruction of faults in elastic half space. *Inverse Problems & Imaging*, 13(3):479–511, 2019.
- [24] W. Wendland and E. Stephan. A hypersingular boundary integral method for two-dimensional screen and crack problems. *Archive for Rational Mechanics and Analysis*, 112:363–390, 1990.
- [25] D. Yarotsky. Error bounds for approximations with deep ReLU networks. *Neural Networks*, 94:103–114, 2017.